



# Elementary reaction modeling of solid oxide electrolysis cells: Main zones for heterogeneous chemical/electrochemical reactions



Wenying Li, Yixiang Shi\*, Yu Luo, Ningsheng Cai

Key Laboratory for Thermal Science and Power Engineering of Ministry of Education, Tsinghua University, Beijing 100084, China

## HIGHLIGHTS

- Elementary reaction modeling for solid oxide electrolysis cells.
- Relative performance of H<sub>2</sub>O electrolysis, CO<sub>2</sub> electrolysis and CO<sub>2</sub>/H<sub>2</sub>O co-electrolysis.
- Coupling and competitive effects of heterogeneous chemical reactions and electrochemical reactions.

## ARTICLE INFO

### Article history:

Received 4 February 2014

Received in revised form

23 May 2014

Accepted 29 August 2014

Available online 16 September 2014

### Keywords:

Solid oxide electrolysis cell

Elementary reaction model

Heterogeneous chemical/electrochemical

reaction main zones

Mass and charge transport

## ABSTRACT

A theoretical model of solid oxide electrolysis cells considering the heterogeneous elementary reactions, electrochemical reactions and the transport process of mass and charge is applied to study the relative performance of H<sub>2</sub>O electrolysis, CO<sub>2</sub> electrolysis and CO<sub>2</sub>/H<sub>2</sub>O co-electrolysis and the competitive behavior of heterogeneous chemical and electrochemical reactions. In cathode, heterogeneous chemical reactions exist near the outside surface and the electrochemical reactions occur near the electrolyte. According to the mathematical analysis, the mass transfer flux  $D\nabla c$  determines the main zone size of heterogeneous chemical reactions, while the charge transfer flux  $\sigma\nabla V$  determines the other one. When the zone size of heterogeneous chemistry is enlarged, more CO<sub>2</sub> could react through heterogeneous chemical pathway, and polarization curves of CO<sub>2</sub>/H<sub>2</sub>O co-electrolysis could be prone to H<sub>2</sub>O electrolysis. Meanwhile, when the zone size of electrochemistry is enlarged, more CO<sub>2</sub> could react through electrochemical pathway, and polarization curves of CO<sub>2</sub>/H<sub>2</sub>O co-electrolysis could be prone to CO<sub>2</sub> electrolysis. The relative polarization curves, the ratio of CO<sub>2</sub> participating in electrolysis and heterogeneous chemical reactions, the mass and charge transfer flux and heterogeneous chemical/electrochemical reaction main zones are simulated to study the effects of cathode material characteristics (porosity, particle diameter and ionic conductivity) and operating conditions (gas composition and temperature).

© 2014 Elsevier B.V. All rights reserved.

## 1. Introduction

CO<sub>2</sub>/H<sub>2</sub>O co-electrolysis in solid oxide electrolysis cells (SOECs) is one of the efficient routes to reduce CO<sub>2</sub> emission and to convert and store the renewable power into the form of the chemical energy of hydrocarbon fuel [1–3]. In the cathode, H<sub>2</sub>O and CO<sub>2</sub> electrochemical reductions occur at the triple phase boundary (TPB). The reversible water gas shift (WGS and RWGS) reactions also react on the electrode catalyst (such as nickel):



It is generally believed that CO can be reduced from CO<sub>2</sub> electrolysis and from RWGS reaction, but it is not clear that how much CO is produced from RWGS reaction [3–5]. Two different conclusions can be found in the published experimental studies of CO<sub>2</sub>/H<sub>2</sub>O co-electrolysis: (1) CO<sub>2</sub>/H<sub>2</sub>O co-electrolysis performs almost the same as H<sub>2</sub>O electrolysis, CO is nearly all generated from RWGS reaction [6,7]; (2) CO<sub>2</sub>/H<sub>2</sub>O co-electrolysis performs between H<sub>2</sub>O

\* Corresponding author. Tel./fax: +86 10 62789955.

E-mail address: [shyx@tsinghua.edu.cn](mailto:shyx@tsinghua.edu.cn) (Y. Shi).

electrolysis and CO<sub>2</sub> electrolysis, CO is partial generated from RWGS reaction [3,8]. Ni [2,9] has developed both one-dimensional and two-dimensional thermal-fluid model and studied that the percentage of CO generated from RWGS reaction highly depends on the operating temperature and inlet gas composition of cathode.

Except for temperature and gas composition, we believe the mass and charge transport process in cathode also play an important role on the CO<sub>2</sub> reaction pathway and the relative performance of H<sub>2</sub>O electrolysis, CO<sub>2</sub> electrolysis and CO<sub>2</sub>/H<sub>2</sub>O co-electrolysis. The cathode thickness which influences the transport length has been proved to be one of the factors, through establishing and validating an elementary reaction model in our previous work [10]. It is found that the rate of heterogeneous chemical reactions is about 20–100 times faster than that of electrochemical reactions, and the two kinds of reactions occur in the different zones in cathode as shown in Fig. 1: the heterogeneous chemical reactions mainly react near the outside surface of cathode, while the electrochemical reactions mainly react near the electrolyte. It could be speculated that at the same local reaction site, if the reactant gas doesn't reach the equilibrium, the gas prefers to heterogeneous chemical reactions rather than electrochemical reactions. Thus, for a thick cathode, the electrochemical reaction main zone is far from that of heterogeneous chemical reaction, so that there are sufficient reaction sites for gas reacting first through chemical pathway to reach the equilibrium and then through electrochemical pathway. For CO<sub>2</sub>/H<sub>2</sub>O co-electrolysis, CO<sub>2</sub> can both react through chemical and electrochemical reaction pathways, and the electrochemical performance lies between H<sub>2</sub>O and CO<sub>2</sub> electrolysis. If the cathode is relatively thin, the two zones will overlap and compete with each other. Finally, the gas prefers to participate in chemical reactions first and most of CO<sub>2</sub> reacts through chemical reaction pathway, which causes the performance approaching to H<sub>2</sub>O electrolysis.

In this paper, the objective is to further study the impacts of mass and charge transport on the relative performance of H<sub>2</sub>O electrolysis, CO<sub>2</sub> electrolysis and CO<sub>2</sub>/H<sub>2</sub>O co-electrolysis and the competitive behavior of heterogeneous chemical and electrochemical reactions, which will be beneficial for deeper understanding of the cathode mechanism of CO<sub>2</sub>/H<sub>2</sub>O co-electrolysis, cell design and optimizations.

**Table 1**  
Heterogeneous reaction mechanism on Ni-based catalysts.

Reaction	A (cm, mol, s) <sup>a</sup>	n <sup>a</sup>	E (kJ mol <sup>-1</sup> ) <sup>a</sup>
<b>Adsorption &amp; desorption</b>			
1 <sup>f</sup> H <sub>2</sub> (g) + (Ni) → H(Ni) + H(Ni)	1.000 × 10 <sup>-02b</sup>	0.0	0.00
1 <sup>r</sup> H(Ni) + H(Ni) → (Ni) + (Ni) + H <sub>2</sub> (g)	2.545 × 10 <sup>+19</sup>	0.0	81.21
2 <sup>f</sup> O <sub>2</sub> (g) + (Ni) + (Ni) → O(Ni) + O(Ni)	1.000 × 10 <sup>-02b</sup>	0.0	0.00
2 <sup>r</sup> O(Ni) + O(Ni) → (Ni) + (Ni) + O <sub>2</sub> (g)	4.283 × 10 <sup>+23</sup>	0.0	474.95
3 <sup>f</sup> H <sub>2</sub> O(g) + (Ni) → H <sub>2</sub> O(Ni)	0.100 × 10 <sup>-00b</sup>	0.0	0.00
3 <sup>r</sup> H <sub>2</sub> O(Ni) → (Ni) + H <sub>2</sub> O(g)	3.732 × 10 <sup>+12</sup>	0.0	60.79
4 <sup>f</sup> CO <sub>2</sub> (g) + (Ni) → CO <sub>2</sub> (Ni)	1.000 × 10 <sup>-05b</sup>	0.0	0.00
4 <sup>r</sup> CO <sub>2</sub> (Ni) → (Ni) + CO <sub>2</sub> (g)	6.447 × 10 <sup>+07</sup>	0.0	25.98
5 <sup>f</sup> CO(g) + (Ni) → CO(Ni)	5.000 × 10 <sup>-02b</sup>	0.0	0.00
5 <sup>r</sup> CO(Ni) → (Ni) + CO(g)	3.563 × 10 <sup>+11</sup>	0.0	111.27
	θ <sub>CO(s)</sub>		-50.00 <sup>c</sup>
<b>Surface reactions</b>			
6 <sup>f</sup> H(Ni) + O(Ni) → OH(Ni) + (Ni)	5.000 × 10 <sup>+22</sup>	0.0	97.90
6 <sup>r</sup> OH(Ni) + (Ni) → H(Ni) + O(Ni)	1.781 × 10 <sup>+21</sup>	0.0	36.09
7 <sup>f</sup> H(Ni) + OH(Ni) → H <sub>2</sub> O(Ni) + (Ni)	3.000 × 10 <sup>+20</sup>	0.0	42.70
7 <sup>r</sup> H <sub>2</sub> O(Ni) + (Ni) → H(Ni) + OH(Ni)	2.271 × 10 <sup>+21</sup>	0.0	91.76
8 <sup>f</sup> OH(Ni) + OH(Ni) → H <sub>2</sub> O(Ni) + O(Ni)	3.000 × 10 <sup>+21</sup>	0.0	100.00
8 <sup>r</sup> H <sub>2</sub> O(Ni) + O(Ni) → OH(Ni) + OH(Ni)	6.373 × 10 <sup>+23</sup>	0.0	210.86
9 <sup>f</sup> CO(Ni) + O(Ni) → CO <sub>2</sub> (Ni) + (Ni)	2.000 × 10 <sup>+19</sup>	0.0	123.60
	θ <sub>CO(s)</sub>		-50.00 <sup>c</sup>
9 <sup>r</sup> CO <sub>2</sub> (Ni) + (Ni) → CO(Ni) + O(Ni)	4.653 × 10 <sup>+23</sup>	-1.0	89.32

<sup>a</sup> Arrhenius parameters for the rate constant written in the form:  $k = AT^n \exp(-E/RT)$ .

<sup>b</sup> Sticking coefficient.

<sup>c</sup> Coverage dependent activation energy.

The elementary reaction model of SOECs developed and validated in our previous work [10] continues to be used in this simulation. The sizes of the heterogeneous chemical/electrochemical reaction main zones are quantified according to the mathematical analysis. The effects of material characteristics of cathode and operating conditions of SOECs are studied in details. Here, the microstructure including porosity  $\epsilon_{ca}$  and particle diameter  $d_{ca}$ , and the ionic conductivity  $\sigma_{ion,ca}$  are chosen as the typical parameters of material characteristics. In addition, as the important operating parameters, the effects of temperature  $T$  and gas composition are also discussed.

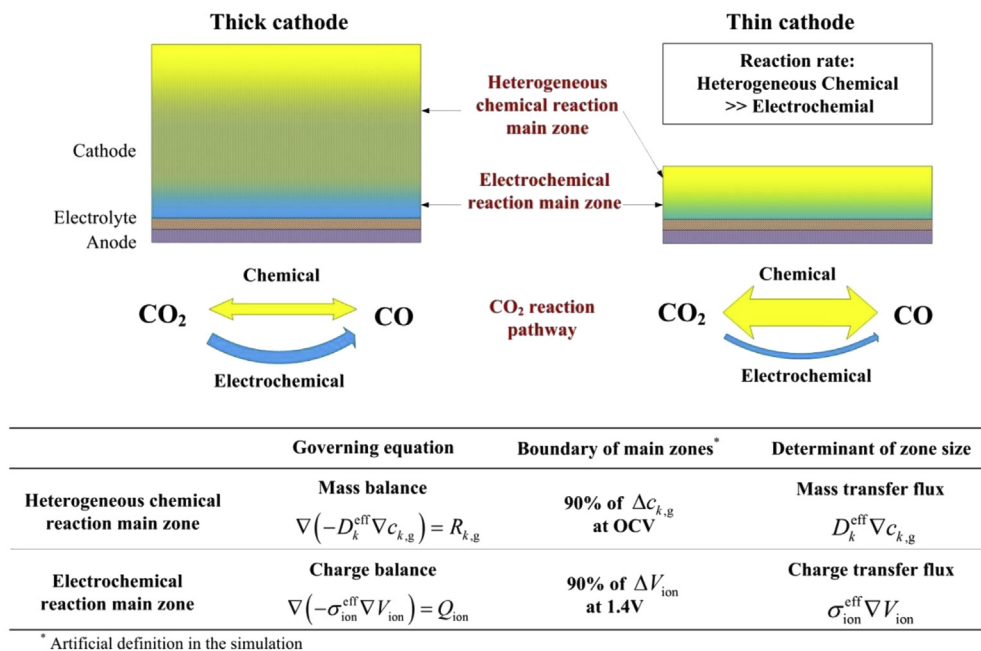


**Fig. 1.** Heterogeneous chemical/electrochemical reaction main zones, CO<sub>2</sub> reaction pathway and mathematical analysis of the two zones.

**Table 2**

Summary of the governing equations of the model. Details can be found in Refs. [10–12].

**Cathode heterogeneous chemistry**

The reaction rate constant of surface reactions and desorption reactions the Arrhenius form

$$k_i = A_i T^{n_i} \exp\left(-\frac{E_i}{RT}\right) \prod_{k=1}^{K_s+K_s} \theta_k^{\mu_k} \exp\left(-\frac{\epsilon_{ki} \theta_k}{RT}\right) \quad (4)$$

The reaction rate constant of adsorption reactions

$$k_i = a_i T^{b_i} \exp\left(-\frac{d_i}{RT}\right) \frac{1}{\Gamma^\gamma} \sqrt{\frac{RT}{2\pi W}} \quad (5)$$

**Cathode electrochemistry**

The current source

$$Q_{ca} = 2F \left( k_{ec} c_{O(Ni)} c_{(YSZ)} - k_{-ec} c_{O^{2-}(YSZ)} c_{(Ni)} \right) S_{TPB} \quad (6)$$

The forward electrochemical reaction rates

$$k_{ec} = \frac{i_0}{FS_{TPB} c_{O(Ni)}^0 c_{(YSZ)}^0} \exp\left[-2(1-\alpha) \frac{F\eta_{ca}}{RT}\right] \quad (7)$$

The reverse electrochemical reaction rates

$$k_{-ec} = \frac{i_0}{FS_{TPB} c_{O^{2-}(YSZ)}^0 c_{(Ni)}^0} \exp\left(-2\alpha \frac{F\eta_{ca}}{RT}\right) \quad (8)$$

The cathode overpotential

$$\eta_{ca} = V_{elec,ca} - V_{ion,ca} - V_{ref,ca} \quad (9)$$

**Reaction area**

The TPB active area per unit volume

$$S_{TPB} = \frac{\pi \sin^2 \theta r_{ep}^2 n_t n_{ep} n_{ip} Z_{ep} Z_{ip} P_{ep} P_{ip}}{Z} \quad (10)$$

The effective Ni surface area per unit volume

$$S_{Ni} = \pi r_{ep}^2 n_t n_{ep} \left( 4 - \frac{\sin^2 \theta n_{ip} Z_{ep} Z_{ip}}{Z} - \frac{\sin^2 \theta n_{ep} Z_{ep} Z_{ep}}{Z} \right) \quad (11)$$

The total number of particles per unit volume

$$n_t = \frac{1 - \epsilon}{\frac{4}{3} \pi r_{ep}^3 (n_{ep} + n_{ip} \alpha^3)} \quad (12)$$

**Charge balance**

The ionic charge equation in cathode

$$\nabla \cdot (-\sigma_{ion,ca}^{eff} \nabla V_{ion,ca}) = Q_{ion,ca} \quad (13)$$

The electronic charge equation in cathode

$$\nabla \cdot (-\sigma_{elec,ca}^{eff} \nabla V_{elec,ca}) = Q_{elec,ca} = -Q_{ion,ca} \quad (14)$$

The ionic charge equation in anode

$$\nabla \cdot (-\sigma_{ion,an}^{eff} \nabla V_{ion,an}) = Q_{ion,an} = -\frac{\beta RT}{4F} \exp\left(-\frac{E_{air}}{RT}\right) (p_{O_2})^{0.25} S_{TPB,an} \cdot \left\{ \frac{c_{O_2}^{TPB}}{c_{O_2}^{bulk}} \exp\left(\frac{2\alpha F\eta_{an}}{RT}\right) - \exp\left[-\frac{2(1-\alpha)F\eta_{an}}{RT}\right] \right\} \quad (15)$$

The electronic charge equation in anode

$$\nabla \cdot (-\sigma_{elec,an}^{eff} \nabla V_{elec,an}) = Q_{elec,an} = -Q_{ion,an} \quad (16)$$

The ionic charge equation in electrolyte

$$\nabla \cdot (-\sigma_{ion,el}^{eff} \nabla V_{ion,el}) = 0 \quad (17)$$

The anode overpotential

$$\eta_{an} = V_{elec,an} - V_{ion,an} - V_{ref,an} \quad (18)$$

**Mass balance**

The mass balance equation in porous electrode

$$\nabla \cdot (-D_k^{eff} \nabla c_{k,g}) = R_{k,g} \quad (19)$$

The effective diffusivity of gas species  $k$ 

$$D_k^{eff} = \left( \frac{1}{D_{k,mole}^{eff}} + \frac{1}{D_{k,kn}^{eff}} \right)^{-1} \quad (20)$$

The effective molecular diffusion coefficient

$$D_{k,mole}^{eff} = \left[ \frac{1 - x_k}{\sum_{j \neq k}^n (x_j / D_{k,j}^{eff})} \right] \quad (21)$$

The effective binary molecular diffusion coefficient

$$D_{k,j}^{eff} = \frac{0.00101 \epsilon T^{1.75} (1/M_k + 1/M_j)^{1/2}}{\tau p (V_k^{1/3} + V_j^{1/3})^2} \quad (22)$$

The effective Knudsen diffusion coefficient

$$D_{k,kn}^{eff} = \frac{4\epsilon \bar{r}}{3\tau} \sqrt{\frac{8RT}{\pi M_k}} \quad (23)$$

The source terms of both gas and surface species in fuel electrode

$$R_k = S^{eff} \cdot \sum_{i=1}^{N+2} (\nu_{ki}'' - \nu_{ki}') k_i \prod_{k=1}^{K_s+K_s} c_k^{\nu_{ki}'} \quad (24)$$

The source terms in anode

$$R_{O_2} = \frac{Q_{elec,an}}{4F} \quad (25)$$

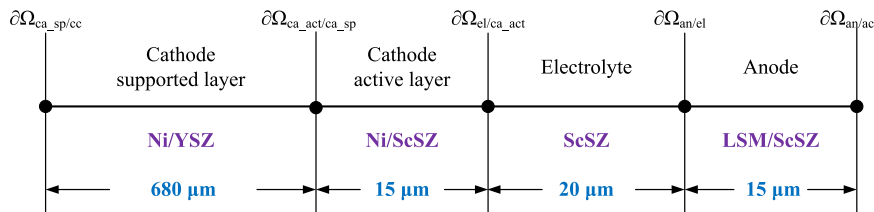


Fig. 2. Simplified modeling geometry and materials.

## 2. Model development, experiment and model validation

A one-dimensional elementary reaction model of SOECs using the finite element commercial software COMSOL Multiphysics is developed and described in details in our previous work [10–13]. This model couples with elementary heterogeneous reactions [14,15], electrochemical reactions [16,17], charge balance [18–20] and mass balance considering molecular diffusion and Knudsen diffusion [14,21–23]. A heterogeneous reaction mechanism on Ni-based catalysts simplified from the works of Deutschmann's group [15,24] is used and listed in Table 1. The effective TPB area and Ni surface area are calculated by the particle coordination number theory in binary random packing of spheres and the percolation theory [20,21]. The governing equations of the model are summarized in Table 2.

Cathode supported button cells made by Shanghai Institute of Ceramics Chinese Academy of Sciences were tested by a button cell reactor and measurement system [11,12]. The simplified modeling geometry and materials are shown in Fig. 2. This SOEC model was validated with the polarization curves of H<sub>2</sub>O electrolysis, CO<sub>2</sub> electrolysis and CO<sub>2</sub>/H<sub>2</sub>O co-electrolysis with different compositions at 700 °C [10]. In this paper, all the model parameters are the same as the Ref. [10] and would not be changed.

## 3. Simulation conditions and parameters definition

Table 3 summaries the main simulation conditions used in the model. The cathode porosity  $\epsilon_{ca}$  and cathode particle diameter  $d_{ca}$

Table 3  
Simulation conditions of the model.

Parameter	Value, Unit
<b>Microstructure</b>	
Porosity of cathode, $\epsilon_{ca}$	
Experiment value	0.335 [10]
Simulation value	0.3–0.6
Particle diameter of cathode, $d_{ca}$ (assumption: particle diameter = pore diameter)	
Experiment value	0.60 [10] $\mu\text{m}$
Simulation value	0.6–1.2 $\mu\text{m}$
<b>Ionic conductivity of cathode, <math>\sigma_{ion,ca}</math></b>	
Validation value	YSZ: $3.34 \times 10^4 \cdot \exp(-10300/T^{-1})$ [25] $\text{S m}^{-1}$ ScSZ: $6.92 \times 10^4 \cdot \exp(-9681/T^{-1})$ [11] $\text{S m}^{-1}$
Simulation value	Validation value $\times 1.0$ –4.0
<b>Gas composition</b>	
Cathode	
Oxidant:reductant	H <sub>2</sub> O/H <sub>2</sub> H <sub>2</sub> O/H <sub>2</sub> /CO <sub>2</sub> /CO    CO <sub>2</sub> /CO
4:1	80/20    40/10/40/10    80/20
3:2	60/40    30/20/30/20    60/40
1:1	50/50    25/25/25/25    50/50
2:3	40/60    20/30/20/30    40/60
1:4	20/80    10/40/40/10    20/80
Anode	O <sub>2</sub> /N <sub>2</sub> = 21/79
Temperature	700–900 °C
Pressure	1.0 bar

are changed in the ranges of 0.3–0.6 and 0.6–1.2  $\mu\text{m}$ , respectively. Here, the particle diameters of ionic and electronic conductors in electrodes are assumed to be the same and equal to the pore diameter [23,26]. The cathode ionic conductivity  $\sigma_{ion,ca}$  is artificially multiplied by a factor ranged from 1.0 to 4.0. For comparison, the cathode gas compositions of H<sub>2</sub>O electrolysis, CO<sub>2</sub> electrolysis and CO<sub>2</sub>/H<sub>2</sub>O co-electrolysis are given as the same ratio of oxidant and reductant which is varied from 4:1 to 1:4. The ratio of H<sub>2</sub>O and CO<sub>2</sub> and ratio of H<sub>2</sub> and CO for co-electrolysis are all fixed as 1. Air is supplied in the anode. The temperature is changed from 700 °C to 900 °C, while pressure is kept at 1.0 bar.

Quantifying the size of the heterogeneous chemical/electrochemical reaction main zones could supply a more legible and visual way to analyze. As shown in Fig. 1 and Table 2, the heterogeneous chemistry is mainly calculated by the mass balance equation (Eq. (19)), and the information of reaction rates are all inside the sources  $R$  (Eq. (24)). Thus, the variation speed of  $c$ , the mass transfer flux  $D\nabla c$ , could signify the overall reaction rate of heterogeneous chemistry. Similarly, the electrochemistry is mainly calculated by the charge balance equation (Eq. (13)), and its source  $Q$  involves in the electrochemical reaction rates (Eqs. (6)–(8)). So the charge transfer flux  $\sigma\nabla V$ , the term in the parentheses of Eq. (13), denotes the overall reaction rate of electrochemistry. We artificially define that the boundary of main zone of chemical reactions is the location where  $c$  has been 90% changed without current (at OCV), meanwhile the boundary of electrochemical reactions is the location where  $V$  has been 90% changed with current (for example at 1.4 V). This specific value 90% doesn't have any physical meaning here, and can be any other values like 95% or 85%. This value is only used to quantify the zone size and further to compare and analysis its variation.

The mass transfer flux for all the gas species H<sub>2</sub>O, H<sub>2</sub>, CO<sub>2</sub>, CO is all the same on the basis of mathematics. Besides, according to the gas distribution in cathode calculated in Fig. 6 of Ref. [10], it was shown that the heterogeneous chemical reactions on Ni product CO<sub>2</sub> and H<sub>2</sub> but consume CO and H<sub>2</sub>O at 700 °C; the electrochemical reactions product CO and H<sub>2</sub> but consume CO<sub>2</sub> and H<sub>2</sub>O. Thus, CO<sub>2</sub> and CO show the opposite behaviors on these two kinds of reactions, and the concentration of CO<sub>2</sub> is chosen to quantify the zone here. As shown in Fig. 3(a), the heterogeneous chemical reaction main zone is quantified as the zone from the outside surface of cathode to the location with 90%  $\Delta c_{\text{CO}_2}$  at OCV. On the other hand, the ionic transport is much slower than electronic transport and limits the charge transport, so that the ionic potential is used to quantify the zone. The electrochemical reaction main zone includes the zone from the electrolyte to the location with 90%  $\Delta V_{\text{ion}}$  at 1.4 V, as shown in Fig. 3(b).

In order to clear how much CO<sub>2</sub> reacts through chemical or electrochemical reaction pathway, the ratio of the variation of CO<sub>2</sub> concentration reduced by electrolysis  $\Delta c_{\text{CO}_2, \text{electrochemical}}$  and the variation caused by chemical reactions  $\Delta c_{\text{CO}_2, \text{chemical}}$  is quantified as follows and expressed in Fig. 3(a):

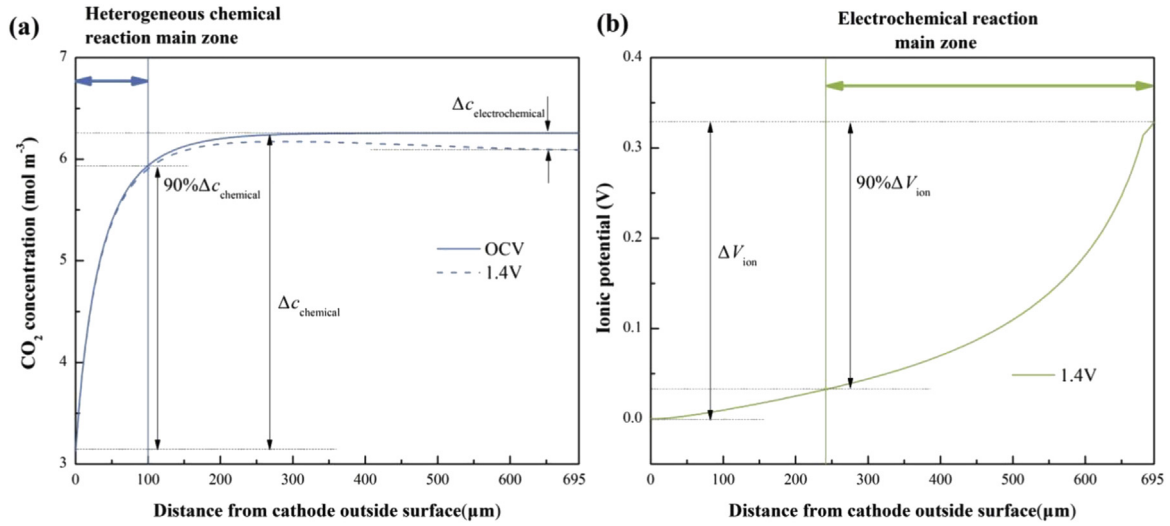


Fig. 3. Quantification of the sizes of heterogeneous chemical/electrochemical reaction main zones.

$$r_{er/cr} = \frac{\Delta c_{CO_2, \text{electrochemical}}}{\Delta c_{CO_2, \text{chemical}}} = \frac{c_{CO_2, \text{el}}(\text{OCV}) - c_{CO_2, \text{el}}(1.4\text{V})}{c_{CO_2, \text{el}}(\text{OCV}) - c_{CO_2, \text{cc}}(\text{OCV})} \quad (26)$$

$\Delta c_{CO_2, \text{electrochemical}}$  is approximately considered as the difference of concentration at the boundary of electrolyte  $c_{CO_2, \text{el}}$  at OCV and 1.4 V. Besides,  $\Delta c_{CO_2, \text{chemical}}$  could be equal to the difference of concentration at the boundary of electrolyte  $c_{CO_2, \text{el}}$  and concentration at the boundary of cathode surface  $c_{CO_2, \text{cc}}$  at OCV.

## 4. Results and discussion

### 4.1. Effect of microstructure: porosity and particle diameter

#### 4.1.1. Polarization curves and $r_{er/cr}$

Fig. 4 represents and compares the polarization curves of  $H_2O$  electrolysis,  $CO_2$  electrolysis and  $CO_2/H_2O$  co-electrolysis with different cathode porosities  $\varepsilon_{ca}$  and particle diameters  $d_{ca}$ . The temperature is fixed as 700 °C, and the ratio of oxidant and reductant is 1:1. The electrochemical performances of the three

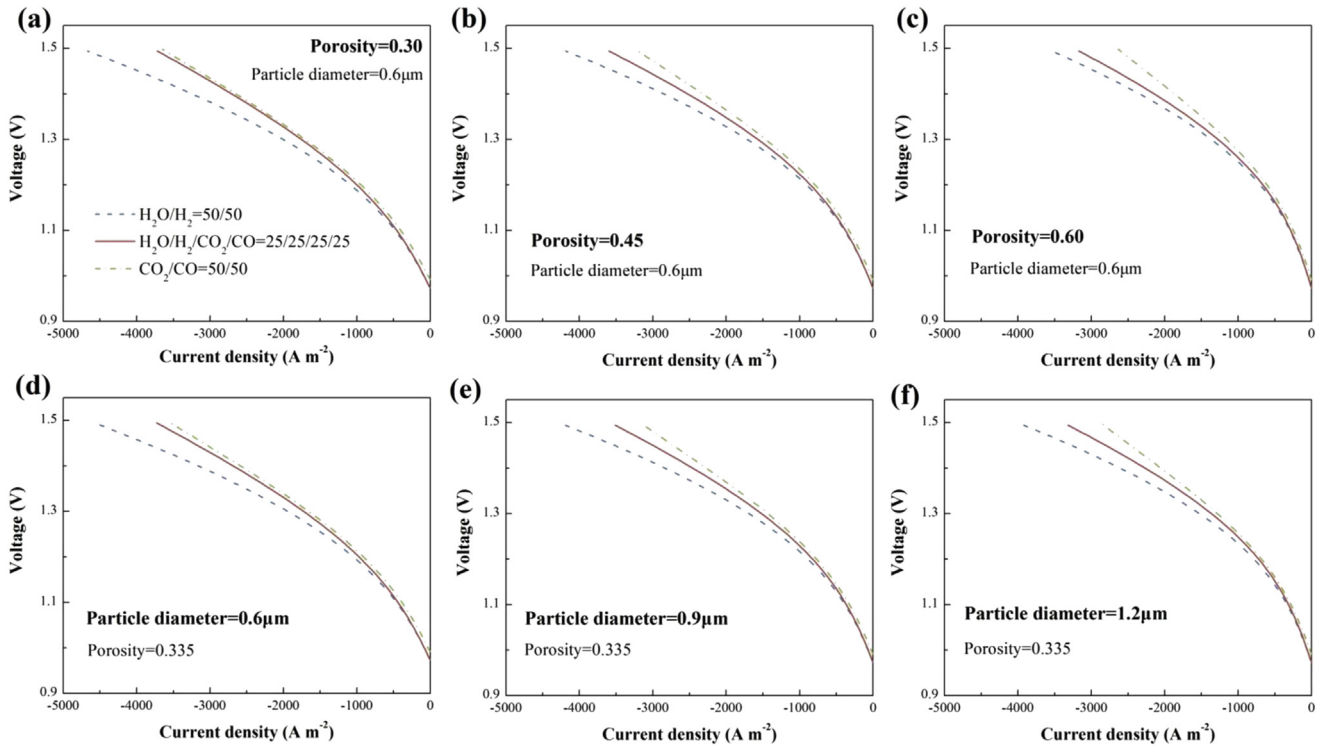


Fig. 4. Polarization curves comparison of  $H_2O$  electrolysis,  $CO_2$  electrolysis and  $CO_2/H_2O$  co-electrolysis with different cathode porosities (a–c) and different cathode particle diameters (d–f) at 700 °C.

**Table 4**  
Ratio (%) of CO<sub>2</sub> participating in electrolysis and heterogeneous reactions at 1.4 V.

Porosity, $\epsilon_{ca}$ <sup>a</sup>		Particle diameter, $d_{ca}$ <sup>b</sup>		Ionic conductivity, $\sigma_{ion,ca}$ <sup>c</sup>	
0.30	5.24%	0.6 $\mu\text{m}$	4.43%	$\times 1.0$	2.29%
0.35	4.14%	0.7 $\mu\text{m}$	3.73%	$\times 1.5$	2.40%
0.40	3.35%	0.8 $\mu\text{m}$	3.24%	$\times 2.0$	2.47%
0.45	2.76%	0.9 $\mu\text{m}$	2.88%	$\times 2.5$	2.52%
0.50	2.29%	1.0 $\mu\text{m}$	2.60%	$\times 3.0$	2.55%
0.55	1.92%	1.1 $\mu\text{m}$	2.39%	$\times 3.5$	2.58%
0.60	1.61%	1.2 $\mu\text{m}$	2.22%	$\times 4.0$	2.60%
Oxidant:reductant <sup>d</sup>				Temperature, $T$ <sup>e</sup>	
4:1		0.35%		700 °C	2.29%
3:2		0.74%		750 °C	3.60%
1:1		2.29%		800 °C	5.06%
2:3		6.68%		850 °C	6.60%
1:4		12.03%		900 °C	8.23%

<sup>a</sup>  $d_{ca} = 0.6 \mu\text{m}$ , oxidant:reductant = 1:1,  $T = 700 \text{ }^{\circ}\text{C}$ .  
<sup>b</sup>  $\epsilon_{ca} = 0.335$ , oxidant:reductant = 1:1,  $T = 700 \text{ }^{\circ}\text{C}$ .  
<sup>c</sup>  $\epsilon_{ca} = 0.5$ ,  $d_{ca} = 0.6 \mu\text{m}$ , oxidant:reductant = 1:1,  $T = 700 \text{ }^{\circ}\text{C}$ .  
<sup>d</sup>  $\epsilon_{ca} = 0.5$ ,  $d_{ca} = 0.6 \mu\text{m}$ ,  $T = 700 \text{ }^{\circ}\text{C}$ .  
<sup>e</sup>  $\epsilon_{ca} = 0.5$ ,  $d_{ca} = 0.6 \mu\text{m}$ , oxidant:reductant = 1:1.

electrolysis modes all decrease with the enhanced  $\epsilon_{ca}$  in the range of 0.30–0.60, when  $d_{ca}$  is fixed as 0.6  $\mu\text{m}$ , and also decrease with the increasing  $d_{ca}$  from 0.6 to 1.2  $\mu\text{m}$  at the same  $\epsilon_{ca}$  0.335. According to Eqs. (10)–(12) in Table 2, the TPB and Ni surface

areas are both proportional to  $1/d_{ca}$  and  $(1 - \epsilon_{ca})$ ,so that the decreasing variation is mainly attributed to the decreasing reaction active sites per unit volume when  $\epsilon_{ca}$  or  $d_{ca}$  increases. However, to reduce porosity and particle diameter blindly cannot always improve performance due to the gas transport limitation [27].

It is more interesting to observe that the microstructure can not only affect the absolute cell performance, but also can significantly affect the relative cell performance of the three electrolysis modes. The results in Fig. 4(a–c) show that as  $\epsilon_{ca}$  grows, the polarization curve of CO<sub>2</sub>/H<sub>2</sub>O co-electrolysis is gradually close to that of H<sub>2</sub>O electrolysis. As shown in Fig. 4(d–f), increasing  $d_{ca}$  also represents a similar tendency of the relative performance, though the absolute performances all get worse. For CO<sub>2</sub>/H<sub>2</sub>O co-electrolysis, if only H<sub>2</sub>O would participate in electrolysis and CO<sub>2</sub> would be inert in electrolysis, the polarization curves would be similar to that for H<sub>2</sub>O electrolysis, like the experimental results in Refs. [6,7]. If co-electrolysis performs between that of H<sub>2</sub>O and CO<sub>2</sub> electrolysis at the same ratio of oxidant and reductant, it suggests that H<sub>2</sub>O and CO<sub>2</sub> electrolysis both occur in the electrode [3,4]. Thus, we speculate that at the same oxidant and reductant ratio, the tendency of co-electrolysis closing to H<sub>2</sub>O electrolysis denotes more H<sub>2</sub>O and less CO<sub>2</sub> could be reduced by electrolysis and vice versa.

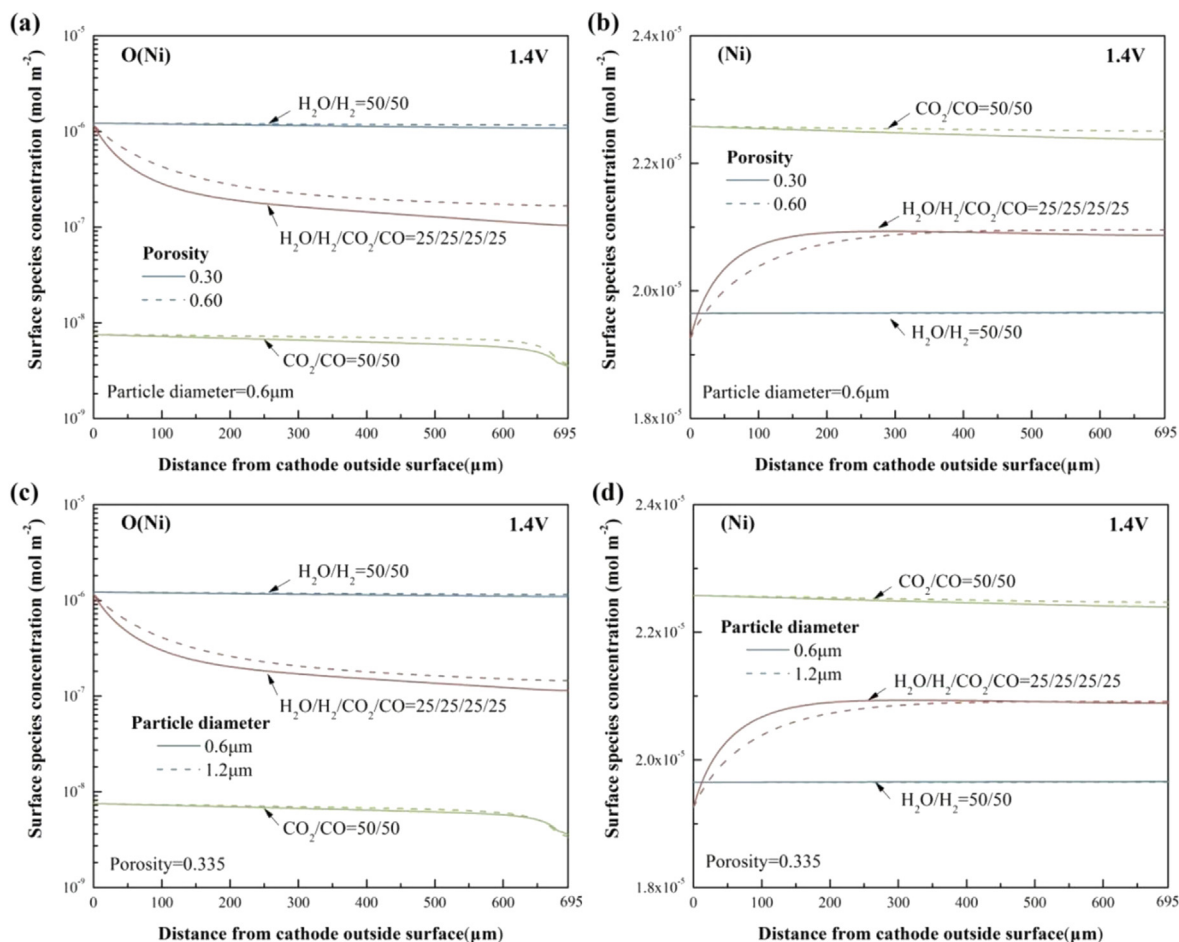


**Fig. 5.** Surface species concentrations of O(Ni) and (Ni) of H<sub>2</sub>O electrolysis, CO<sub>2</sub> electrolysis and CO<sub>2</sub>/H<sub>2</sub>O co-electrolysis with different cathode porosities (a, b) and different cathode particle diameters (c, d) (1.4 V, 700 °C).

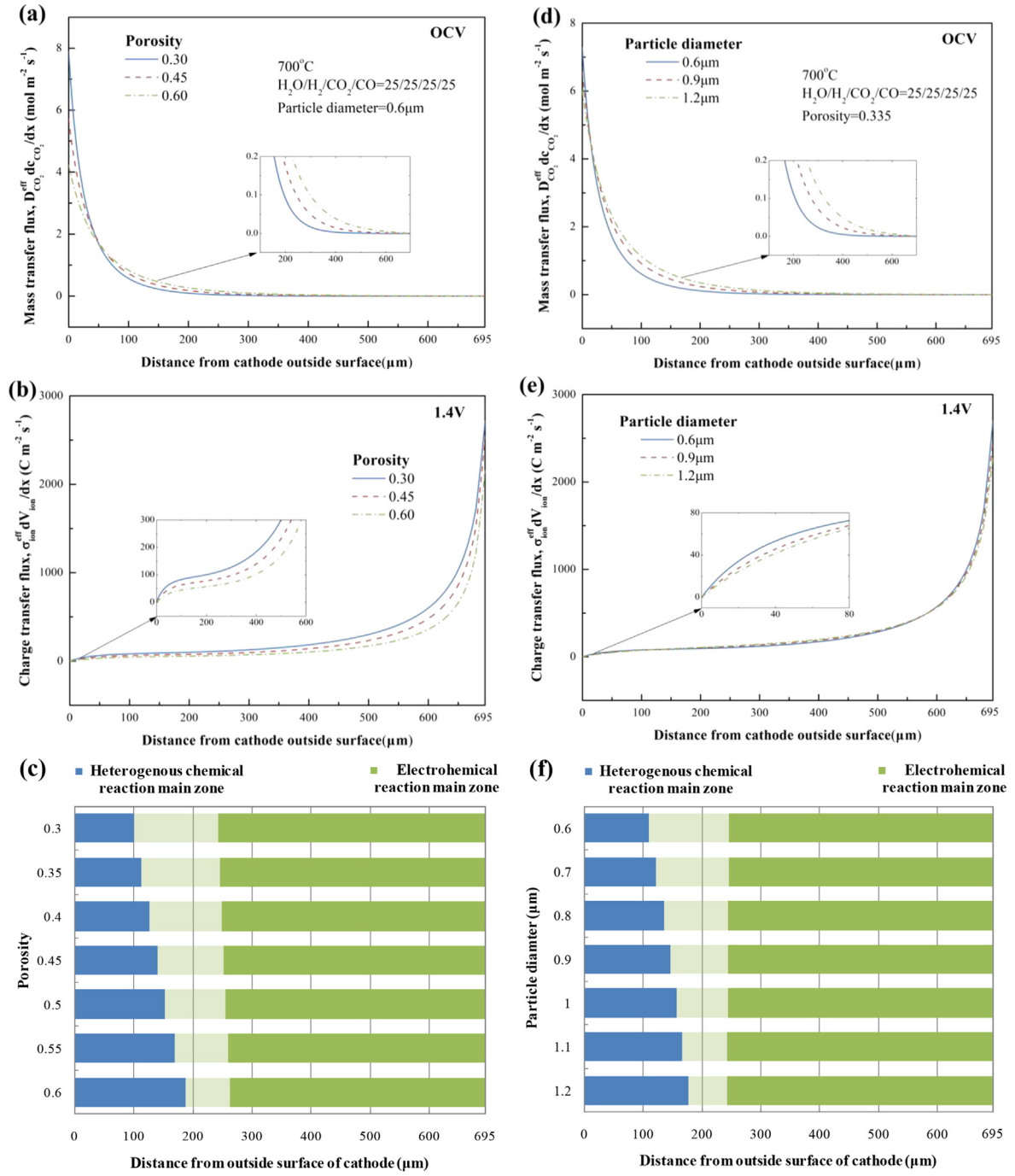


**Fig. 6.** Effects of porosity (a–c) and particle diameter (d–f) on heterogeneous chemical/electrochemical reaction main zones in cathode for  $\text{CO}_2/\text{H}_2\text{O}$  co-electrolysis.

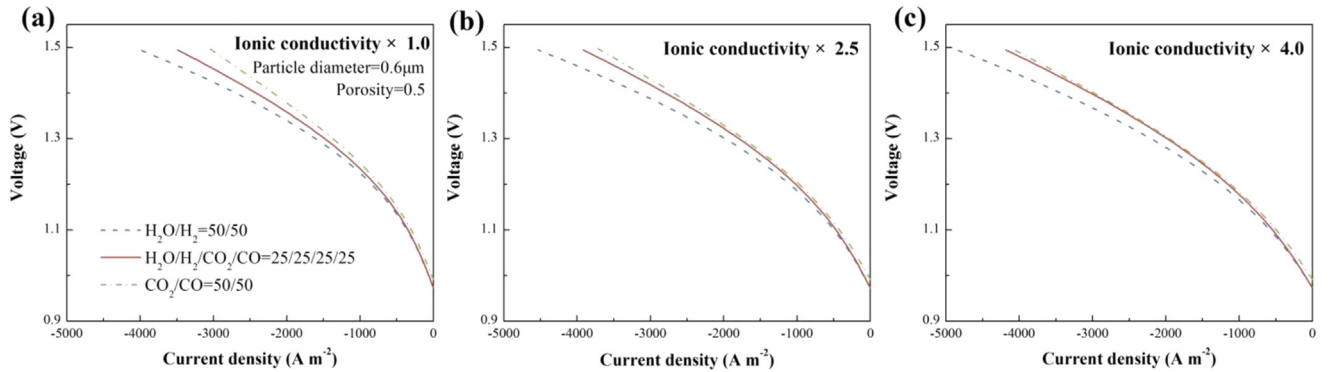


**Fig. 7.** Polarization curves comparison of  $\text{H}_2\text{O}$  electrolysis,  $\text{CO}_2$  electrolysis and  $\text{CO}_2/\text{H}_2\text{O}$  co-electrolysis with cathode ionic conductivity multiplied by a coefficient ranged from 1.0 to 4.0 at  $700^\circ\text{C}$ .

The speculation could be directly proved by the ratio of  $\text{CO}_2$  participating in electrolysis and heterogeneous reactions  $r_{\text{er/cr}}$ , as listed in Table 4. As mentioned before, the reaction rate of heterogeneous chemistry is highly faster than electrochemistry, so the ratio here is a little small. It can be observed that  $r_{\text{er/cr}}$  decreases indeed with the enhanced porosity and particle diameter, which accords with the tendency of relative polarization curves.  $r_{\text{er/cr}}$  at  $\varepsilon_{\text{ca}} = 0.60$  is only about 30% of that at  $\varepsilon_{\text{ca}} = 0.30$ , while  $r_{\text{er/cr}}$  at  $d_{\text{ca}} = 1.2 \mu\text{m}$  is about 50% of that at  $d_{\text{ca}} = 0.6 \mu\text{m}$ . Therefore, these results indicate that when increasing porosity or particle diameter, the electrochemical reaction of  $\text{CO}_2/\text{H}_2\text{O}$  co-electrolysis is prone to  $\text{H}_2\text{O}$  electrolysis, and more  $\text{CO}_2$  reacts through the heterogeneous chemical reaction pathway.

#### 4.1.2. O(Ni) and (Ni) concentrations

According to our previous work [10], as the main surface species of the elementary electrochemical reaction in this model shown in Reaction (27), the surface species concentrations of O(Ni) and (Ni) are proven to be one of the influencing factors which control the relative performance of the three electrolysis modes, after studying all the rate of electrochemical reaction and heterogeneous elementary reactions in details. O(Ni) denotes the O element covered on the Ni surface, and (Ni) denotes the free surface active sites on the Ni surface.

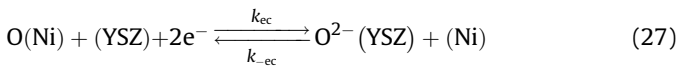


Fig. 5 shows the surface concentrations of O(Ni) and (Ni) at a certain cell voltage of 1.4 V. In the zone near the outside surface of cathode, the variations of both O(Ni) and (Ni) for  $\text{CO}_2/\text{H}_2\text{O}$  co-electrolysis are quite bigger than the other two modes due to the heterogeneous chemical reactions. Moreover, the porosity and particle diameter also both have bigger influence on the O(Ni) and (Ni) concentrations in co-electrolysis mode than that in the other two modes. When  $\varepsilon_{\text{ca}}$  or  $d_{\text{ca}}$  increases, the average O(Ni) concentration of  $\text{CO}_2/\text{H}_2\text{O}$  co-electrolysis increases and the average (Ni) concentration decreases, and both of their curves become close to the curves of  $\text{H}_2\text{O}$  electrolysis. Thus, although the absolute forward and reverse electrochemical reaction rates ( $k_{\text{ec}}$ ,  $k_{-\text{ec}}$ ) of the three modes all decrease, the relative electrochemical performance of  $\text{CO}_2/\text{H}_2\text{O}$  co-electrolysis is prone to that of  $\text{H}_2\text{O}$  electrolysis, after multiplying the rate by the surface concentrations of O(Ni) and (Ni) (Eq. (6)).

#### 4.1.3. The sizes of heterogeneous chemical/electrochemical reaction main zones

O(Ni) and (Ni) concentrations offer an explanation at a micro and elementary level, moreover, the analysis of heterogeneous chemical/electrochemical reaction main zones can interpret this phenomena at a macro and more legible way.

Fig. 6 represents the effects of porosity and particle diameter on mass and charge transfer flux which are the determinant parameters of the size of two zones as analyzed in Section 3, and summarizes the sizes of heterogeneous chemical/electrochemical reaction main zones in a bar chart. The blue (in the web version) column denotes the heterogeneous chemical reaction main zone while the green (in the web version) denotes the electrochemical one. The results indicate that the microstructure strongly affects the main zone size of heterogeneous chemical reaction, but slightly affects that of electrochemical reaction. The size of chemical zone increases from 101  $\mu\text{m}$  to 188  $\mu\text{m}$  when  $\varepsilon_{\text{ca}}$  increases from 0.30 to 0.60, while the size of electrochemical zone is only reduced 20  $\mu\text{m}$ . When  $d_{\text{ca}}$  is varied in the range of 0.6–1.2  $\mu\text{m}$ , the size of chemical

zone is enlarged from 110  $\mu\text{m}$  to 178  $\mu\text{m}$ , while the size of electrochemical zone slightly increases only 3  $\mu\text{m}$ .

From Fig. 6(a) and (c), the mass transfer flux  $D_{\text{CO}_2}^{\text{eff}} \nabla c_{\text{CO}_2}$  falls down quickly with the distance from outside surface of cathode and

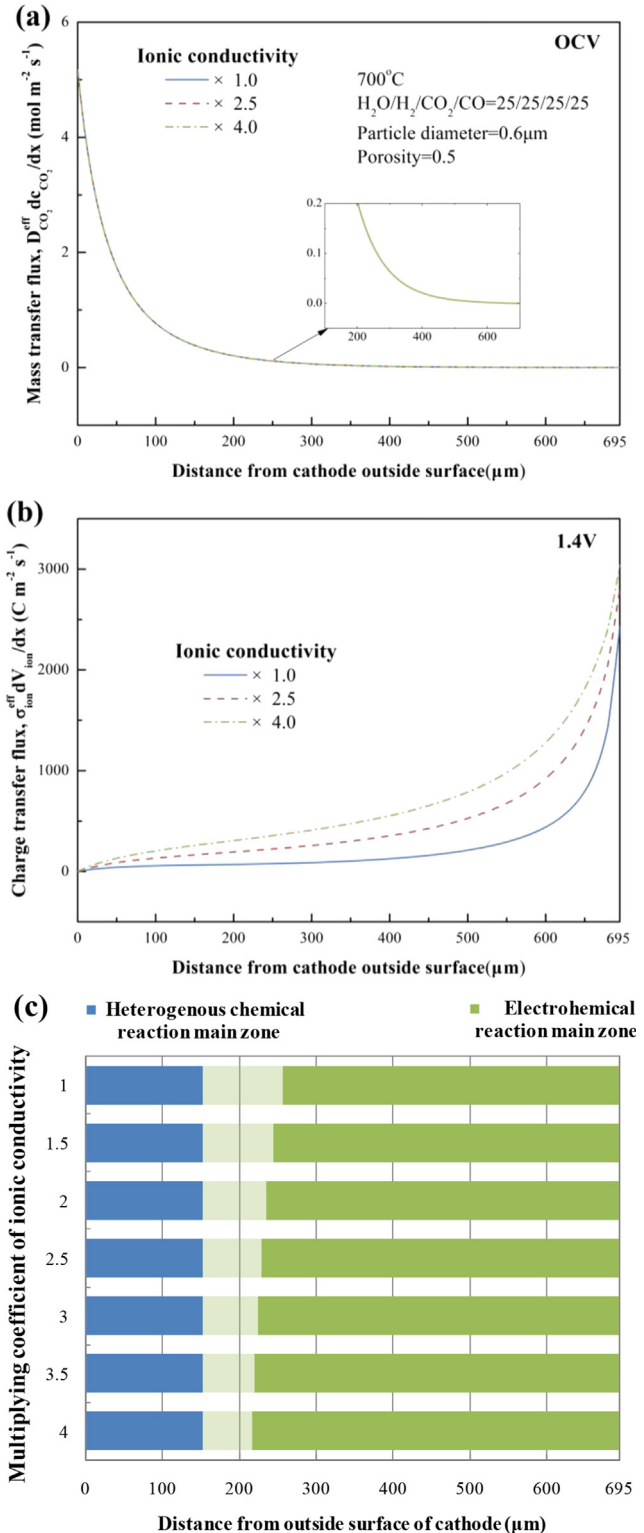


Fig. 8. Effects of cathode ionic conductivity on heterogeneous chemical/electrochemical reaction main zones in cathode for  $\text{CO}_2/\text{H}_2\text{O}$  co-electrolysis.

then gradually approaches to zero, without the influence of electricity. The zero here signifies the gas concentration would not change and no heterogeneous chemical reactions would occur. When  $\varepsilon_{ca}$  or  $d_{ca}$  increases, the effective diffusivity of gas species  $D_{eff}$  will increase and the mass transport process is improved according to Eqs. (20)–(23), although the original mass transfer rate at the cathode surface decreases.  $\varepsilon_{ca}$  could affect both the binary molecular diffusion and Knudsen diffusion coefficient while  $d_{ca}$  could only affect the latter coefficient, and then  $\varepsilon_{ca}$  and  $d_{ca}$  both influence the molecular diffusion coefficient and further the gas diffusivity through changing the gas molar fraction  $x$ . That's why zone size of heterogeneous chemical reactions increases with  $\varepsilon_{ca}$  and  $d_{ca}$ , and the variation of zone size caused by  $\varepsilon_{ca}$  is bigger than that caused by  $d_{ca}$ , when  $\varepsilon_{ca}$  and  $d_{ca}$  are both doubled.

In addition, the results in Fig. 6(b) and (e) show that the charge transfer flux  $\sigma_{ion}^{eff} \nabla V_{ion}$  also drops down as expected when away from electrolyte. The rate of descent for charge transfer is slower than that for mass transfer, so that the main zone of electrochemistry is larger than that of chemistry. As  $\varepsilon_{ca}$  or  $d_{ca}$  increases, the TPB active area per unit volume  $S_{TPB}$  decreases and charge transfer is affected according to Eq. (15), which slightly enlarges the zone size of electrochemistry like the small variation in Fig. 6(f). Moreover, the porosity is related to the effective ionic conductivity  $\sigma_{eff}$ :

$$\sigma_{eff} = (1 - \varepsilon)\sigma \quad (28)$$

The impact of ionic conductivity would be larger than that of reaction active sites, so that charge transfer flux obviously decreases with  $\varepsilon_{ca}$  and electrochemistry reacts in a smaller reaction zone.

On the whole, as  $\varepsilon_{ca}$  or  $d_{ca}$  increases, the mass transport is obviously improved and the main zone of heterogeneous chemical reactions is expanded, so that more  $CO_2$  reacts through chemical reaction pathway for  $CO_2/H_2O$  co-electrolysis and then the relative cell performance is prone to  $H_2O$  electrolysis.

#### 4.2. Effect of ionic conductivity

The cathode ionic conductivity  $\sigma_{ion,ca}$  is another typical material parameters. Fig. 7 compares the relative polarization curves of  $H_2O$  electrolysis,  $CO_2$  electrolysis and  $CO_2/H_2O$  co-electrolysis and Fig. 8 shows the heterogeneous chemical/electrochemical reaction main zones, with different multiplying coefficients of ionic conductivity at the same ratio of oxidant and reductant. The absolute cell performances of the three electrolysis modes are all enhanced

by improving the ionic conduction or charge transport as expected. It can be observed that the ionic conductivity also plays an important role on the relative performance of the three electrolysis modes. When  $\sigma_{ion,ca}$  increases, the curve of co-electrolysis gradually approaches to that of  $CO_2$  electrolysis, and more  $CO_2$  participates in electrolysis as shown in Table 4  $r_{er/cr}$  at 1.4 V increases from 2.29% to 2.60% when ionic conductivity grows to 4 times larger. This could be because that when the electrochemical reaction rate increases, the competitive ability of electrochemistry is relatively improved, so that more  $CO_2$  reacts through the electrochemical pathway.

Besides,  $\sigma_{ion,ca}$  almost has no effect on mass transfer flux at OCV as shown in Fig. 8(a), so that the zone size of heterogeneous chemical reaction doesn't change with  $\sigma_{ion,ca}$  in Fig. 8(c). The results also show that  $\sigma_{ion,ca}$  significantly increases the charge transfer flux and expands the electrochemical reaction main zone. As  $\sigma_{ion,ca}$  increases to 4 times, the size of electrochemical main zone is enlarged from 438  $\mu m$  to 477  $\mu m$ . Therefore, the results above indicate that when the zone of electrochemistry is enlarged, more  $CO_2$  for  $CO_2/H_2O$  co-electrolysis could be electrolyzed, resulting in a polarization curve approaching to the curve of  $CO_2$  electrolysis.

#### 4.3. Effect of gas composition

If only the ratios of oxidant and reductant are the same, the polarization curves for the three electrolysis modes could be comparable. At a fixed ratio of oxidant and reductant, increasing  $H_2O/CO_2$  makes the performance close to  $H_2O$  electrolysis as expected. Thus the  $H_2O/CO_2$  is kept as 1 and only the different oxidant:reductants are discussed in details in this section. The relative polarization curves and heterogeneous chemical/electrochemical main zones are displayed in Figs. 9 and 10.

The results in Fig. 9 and Table 4 show that when oxidant:reductant = 4:1, the polarization curves of  $CO_2/H_2O$  co-electrolysis and  $H_2O$  electrolysis are very close, and only 0.35%  $CO_2$  could be electrolyzed at 1.4 V. As oxidant:reductant increases, the relative polarization curve of  $CO_2/H_2O$  co-electrolysis becomes prone to that of  $CO_2$  electrolysis. Meanwhile, the ratio of  $CO_2$  participating in electrolysis and heterogeneous reactions  $r_{er/cr}$  at 1.4 V significantly grows from 0.35% to 12.03%. The tendency of relative polarization curve is in accordance with the variation of  $r_{er/cr}$ . This variation of  $r_{er/cr}$  is much bigger than that caused by material characteristics of cathode in the range of this simulation.

Because the diffusion coefficient of  $H_2$  is higher than the other 3 gas species, bigger  $H_2$  molar fraction in gas composition should

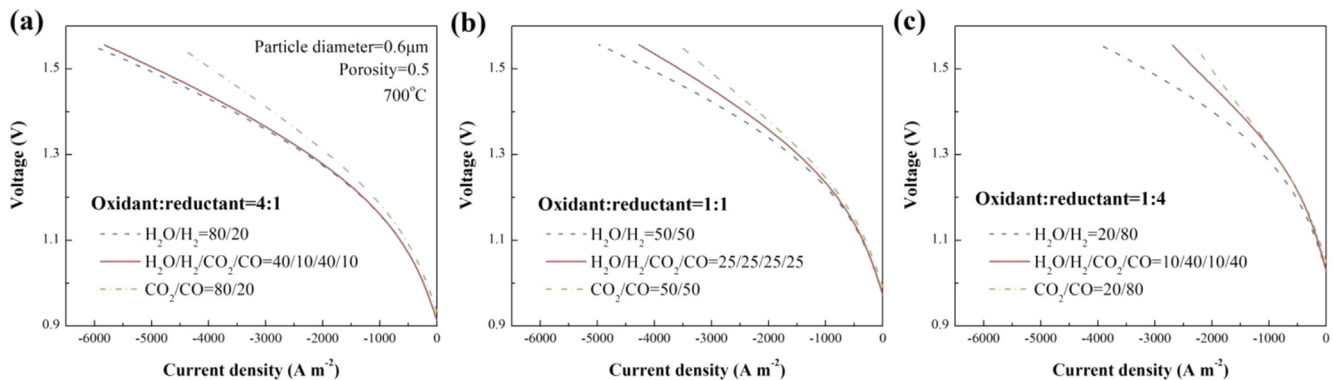


Fig. 9. Polarization curves comparison of  $H_2O$  electrolysis,  $CO_2$  electrolysis and  $CO_2/H_2O$  co-electrolysis with different ratios of oxidant and reductant.

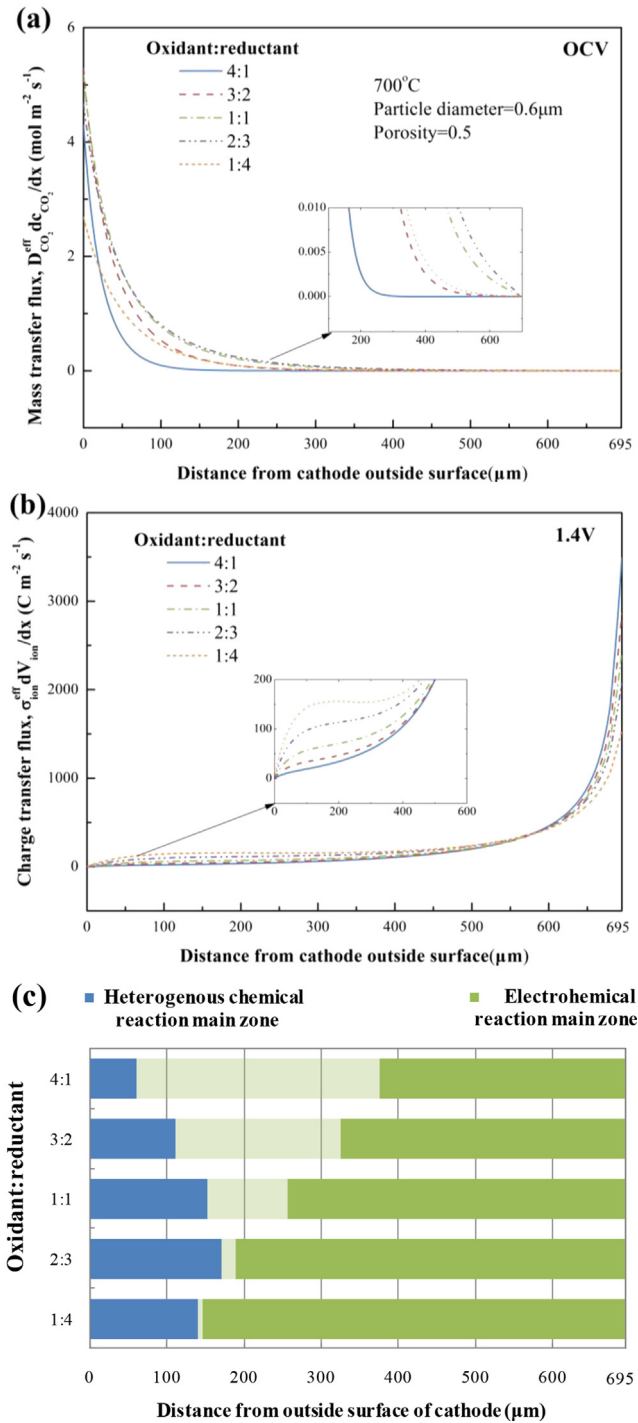


Fig. 10. Effects of the ratio of oxidant and reductant on heterogeneous chemical/electrochemical reaction main zones in cathode for CO<sub>2</sub>/H<sub>2</sub>O co-electrolysis.

Table 5

Effective diffusivity of gas species with different ratios of oxidant and reductant for CO<sub>2</sub>/H<sub>2</sub>O co-electrolysis at OCV.

Oxidant:reductant	$D_{\text{H}_2\text{O}}^{\text{eff}} (10^{-4} \text{ m}^2 \text{ s}^{-1})$		$D_{\text{H}_2}^{\text{eff}} (10^{-4} \text{ m}^2 \text{ s}^{-1})$		$D_{\text{CO}_2}^{\text{eff}} (10^{-4} \text{ m}^2 \text{ s}^{-1})$		$D_{\text{CO}}^{\text{eff}} (10^{-4} \text{ m}^2 \text{ s}^{-1})$	
	$x = 0 \text{ } \mu\text{m}$	$x = 695 \text{ } \mu\text{m}$	$x = 0 \text{ } \mu\text{m}$	$x = 695 \text{ } \mu\text{m}$	$x = 0 \text{ } \mu\text{m}$	$x = 695 \text{ } \mu\text{m}$	$x = 0 \text{ } \mu\text{m}$	$x = 695 \text{ } \mu\text{m}$
4:1	1.03	1.03	2.13	2.10	0.77	0.83	0.863	0.85
3:2	1.10	1.10	2.14	2.04	0.79	0.94	0.913	0.89
1:1	1.14	1.13	2.14	2.01	0.80	0.99	0.946	0.91
2:3	1.17	1.16	2.15	2.01	0.81	0.98	0.987	0.94
1:4	1.23	1.21	2.15	2.08	1.23	0.87	1.107	1.04

contribute to higher effective diffusivity and better mass transfer without regard to reactions. However, from Fig. 10(c), the zone size of heterogeneous chemical reactions doesn't behavior a linear variation. The results in Table 5 show that the original effective diffusivities of the 4 species all increase with the H<sub>2</sub> molar fraction at the cathode surface  $x = 0 \text{ } \mu\text{m}$  at OCV, as the speculation above. However, at the interface of electrolyte and cathode  $x = 695 \text{ } \mu\text{m}$ , the diffusivities of H<sub>2</sub> decrease first and then increase while that of CO<sub>2</sub> increase first and then decrease. This phenomenon is mainly attributed to the heterogeneous chemical reactions, which highly control the variation of gas concentration  $\nabla c$  and then further influence  $D^{\text{eff}}$ . This suggests that to analyze the mass transfer, the diffusivities  $D^{\text{eff}}$  should be taken into consideration, as well as the variation of gas concentration  $\nabla c$  caused by reactions. According to the mass transfer flux in Fig. 10(a), the heterogeneous chemical reactions make  $D_{\text{CO}_2}^{\text{eff}} \nabla c_{\text{CO}_2}$  at oxidant:reductant = 4:1 approaches to zero with the fastest rate and that at oxidant:reductant = 2:3 varies to zero the most slowly. These results mean that the mass transfer is improved when oxidant: reductant varies from 4:1 and 2:3, and then is reduced when oxidant: reductant varies from 2:3 to 1:4, with both diffusivities and reactions taken into account. Therefore, the zone size of heterogeneous chemical reactions is enlarged first and then is reduced as shown in Fig. 10(c).

On the other hand, although the absolute electrochemical reaction rate and the original charge transfer flux at  $x = 695 \text{ } \mu\text{m}$  are reduced with oxidant: reductant, the charge transfer fluxes  $\sigma_{\text{ion}}^{\text{eff}} \nabla V_{\text{ion}}$  of the 5 cases show a totally opposite behavior when  $x$  is close to 0 as shown in Fig. 10(b):  $\sigma_{\text{ion}}^{\text{eff}} \nabla V_{\text{ion}}$  gradually increases with oxidant: reductant. Thus, the zone size of electrochemical reactions significantly increases from 319  $\mu\text{m}$  to 549  $\mu\text{m}$ . Overall, the gas composition both significantly affects the heterogeneous chemical/electrochemical reaction main zones. The influence on electrochemistry is bigger than that on heterogeneous chemistry, so that the overall relative cell performance is prone to CO<sub>2</sub> electrolysis when oxidant:reductant increases.

#### 4.4. Effect of temperature

As another important operating parameter, the effect of temperature on the relative polarization curves of H<sub>2</sub>O electrolysis, CO<sub>2</sub> electrolysis and CO<sub>2</sub>/H<sub>2</sub>O co-electrolysis and on the heterogeneous chemical/electrochemical reaction main zones are displayed in Figs. 11 and 12. Temperature could significantly increase the absolute cell performance of the three electrolysis modes, and also could make the polarization curve of CO<sub>2</sub>/H<sub>2</sub>O co-electrolysis approach to that of CO<sub>2</sub> electrolysis. It should be noted that the polarization curve of CO<sub>2</sub>/H<sub>2</sub>O co-electrolysis in Fig. 11(c) is worse than that of CO<sub>2</sub> electrolysis at lower voltage, just because the OCV of co-electrolysis at 900 °C is higher than that of CO<sub>2</sub> electrolysis. At higher voltage, the curve of co-electrolysis lies between the other two electrolysis modes. The results in Table 4 also represent that

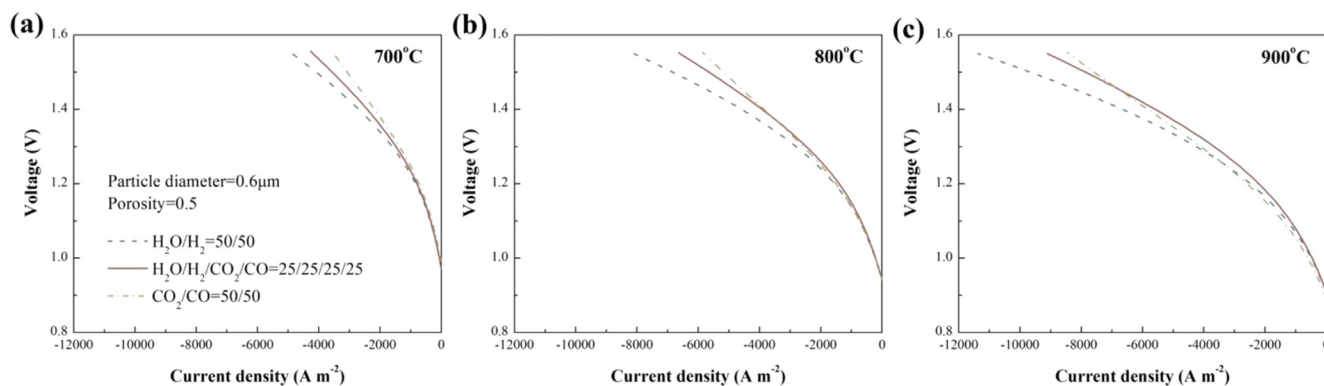


Fig. 11. Polarization curves comparison of  $\text{H}_2\text{O}$  electrolysis,  $\text{CO}_2$  electrolysis and  $\text{CO}_2/\text{H}_2\text{O}$  co-electrolysis with different temperatures.

more  $\text{CO}_2$  could be electrolyzed when increasing temperature.  $r_{\text{er/cr}}$  at 1.4 V significantly grows from 2.29% to 8.23%.

As temperature rises up, diffusion, ionic conduction, rates of chemical and electrochemical reactions could be all enhanced. So according to Fig. 12(a) and (b), although the original  $D_{\text{CO}_2}^{\text{eff}} \nabla c_{\text{CO}_2}$  at  $x = 0 \mu\text{m}$  decreases with temperature, both mass and charge transfer are improved by temperature, especially for charge transfer. The sizes of heterogeneous chemical/electrochemical reaction main zones are both enlarged with temperature, as shown in Fig. 12(c). Besides, the electrochemical reactions are more sensitive to temperature than chemical reactions, so that as temperature rises up, relatively more  $\text{CO}_2$  reacts through electrolysis and then the polarization curve of co-electrolysis is prone to  $\text{CO}_2$  electrolysis.

## 5. Conclusions

In this paper, a one-dimensional elementary reaction model of solid oxide electrolysis cells coupling with the heterogeneous elementary reactions, electrochemical reactions and the mass and charge transport is applied to study the relative performance of  $\text{H}_2\text{O}$  electrolysis,  $\text{CO}_2$  electrolysis and  $\text{CO}_2/\text{H}_2\text{O}$  co-electrolysis and the competitive behavior of heterogeneous chemical and electrochemical reactions. The two kinds of reactions exist in different zones in the cathode of SOECs: the heterogeneous chemical reactions mainly react near the outside surface of cathode, while the electrochemical reactions mainly occur near the electrolyte. The sizes of the heterogeneous chemical/electrochemical reaction main zones are quantified according to the mathematical analysis. The effects of material characteristics of cathode (porosity, particle diameter and ionic conductivity) and operating conditions of SOECs (gas composition and temperature) are studied in details. All the comparisons of the relative cell performance require that the ratios of oxidant and reductant of the three electrolysis modes should be the same.

On the whole, the modeling results indicate that:

- (1) The rate of heterogeneous chemical reactions is about 20–100 times faster than that of electrochemical reactions. At the same local reaction site, if the reactant gas doesn't reach the equilibrium, the gas prefers to heterogeneous chemical reactions rather than electrochemical reactions.
- (2) The mass transfer flux  $D\nabla c$  determines the main zone size of heterogeneous chemical reactions, while the charge transfer flux  $\sigma\nabla V$  determines the main zone size of electrochemical reactions.

- (3) When the mass transfer is improved, the zone size of heterogeneous chemistry could be enlarged, more  $\text{CO}_2$  could react through heterogeneous chemical pathway, and polarization curves of  $\text{CO}_2/\text{H}_2\text{O}$  co-electrolysis could be prone to that of  $\text{H}_2\text{O}$  electrolysis.
- (4) When the charge transfer is improved, the zone size of electrochemistry could be enlarged, more  $\text{CO}_2$  could react through electrochemical pathway, and polarization curves of  $\text{CO}_2/\text{H}_2\text{O}$  co-electrolysis could be prone to that of  $\text{CO}_2$  electrolysis.

Porosity, particle diameter, ionic conductivity, gas composition and temperature have different influence on mass and charge transfer in cathode, and then further differently affect the heterogeneous chemical/electrochemical reaction main zones and the relative cell performance of the three electrolysis modes.

- (1) Porosity and particle diameter strongly affect the mass transfer flux and the zone size of heterogeneous chemical reaction, but slightly affects the charge transfer flux and the zone size of electrochemical reaction. As porosity or particle diameter increases, the mass transport is obviously improved and the main zone of heterogeneous chemical reactions is expanded, so that more  $\text{CO}_2$  reacts through chemical reaction pathway for  $\text{CO}_2/\text{H}_2\text{O}$  co-electrolysis and then the relative cell performance of co-electrolysis is prone to that of  $\text{H}_2\text{O}$  electrolysis.
- (2) Increasing ionic conductivity has no effect on mass transfer flux, but significantly improves charge transfer flux and enlarges the zone size of electrochemical reaction. Thus, the competitive ability of electrochemistry is relatively improved, more  $\text{CO}_2$  could be electrolyzed, and polarization curve of  $\text{CO}_2/\text{H}_2\text{O}$  co-electrolysis approaches to the curve of  $\text{CO}_2$  electrolysis.
- (3) Gas composition shows the biggest influence on the two zones with the parameters in the range of this simulation. The zone size of heterogeneous chemical reactions is enlarged first when oxidant: reductant increases from 4:1 to 2:3, and then is reduced when oxidant: reductant varies from 2:3 to 1:4. The zone size of electrochemical reactions significantly increases with oxidant: reductant. The influence on electrochemistry is bigger than that on heterogeneous chemistry, so that when oxidant: reductant increases, quite more  $\text{CO}_2$  could react through electrochemistry and the overall relative cell performance of co-electrolysis is prone to  $\text{CO}_2$  electrolysis.

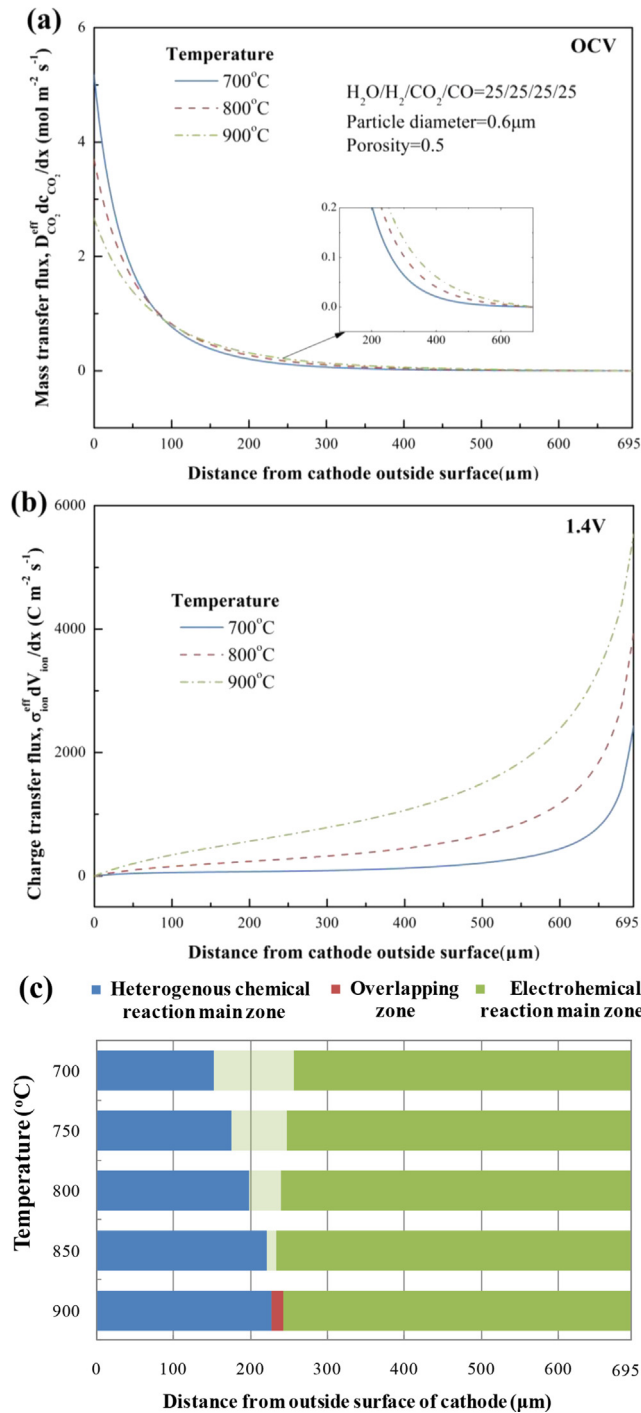


**Fig. 12.** Effect of temperature on heterogeneous chemical/electrochemical reaction main zones in cathode for CO<sub>2</sub>/H<sub>2</sub>O co-electrolysis.

- (4) As temperature rises up, both mass and charge transfer are improved and the sizes of two zones expand. The electrochemical reactions are more sensitive to temperature than chemical reactions, thus when temperature increases, relatively more CO<sub>2</sub> reacts through electrolysis and the polarization curve of co-electrolysis is prone to that of CO<sub>2</sub> electrolysis.

## Acknowledgments

The study was supported by Project 51276098 supported by the Natural Science Foundation of China (NSFC), Project 2014CB249201

supported by the National Basic Research Program of China (973 Program) and Doctoral Fund of Ministry of Education of China (No. 20110002120017).

## References

- [1] C. Graves, S.D. Ebbesen, M. Mogensen, K.S. Lackner, *Renew. Sustain. Energy Rev.* 15 (2011) 1–23.
- [2] M. Ni, *J. Power Sources* 202 (2012) 209–216.
- [3] C. Graves, S.D. Ebbesen, M. Mogensen, *Solid State Ionics* 192 (2011) 398–403.
- [4] S.D. Ebbesen, C. Graves, M. Mogensen, *Int. J. Green. Energy* 6 (2009) 646–660.
- [5] C.M. Stoots, J.E. O'Brien, J.S. Herring, J.J. Hartvigsen, *J. Fuel Cell. Sci. Technol.* 6 (2009) 1–12.
- [6] C. Stoots, J. O'Brien, J. Hartvigsen, *Int. J. Hydrogen Energy* 34 (2009) 4208–4215.
- [7] P. Kim-Lohsoontorn, J. Bae, *J. Power Sources* 196 (2011) 7161–7168.
- [8] W. Li, H. Wang, Y. Shi, N. Cai, *Int. J. Hydrogen Energy* 38 (2013) 11104–11109.
- [9] M. Ni, *Int. J. Hydrogen Energy* 37 (2012) 6389–6399.
- [10] W. Li, Y. Shi, Y. Luo, N. Cai, *J. Power Sources* 243 (2013) 118–130.
- [11] Y. Shi, N. Cai, C. Li, C. Bao, E. Croiset, J. Qian, Q. Hu, S. Wang, *J. Power Sources* 172 (2007) 235–245.
- [12] C. Li, Y. Shi, N. Cai, *J. Power Sources* 195 (2010) 2266–2282.
- [13] Y. Shi, Y. Luo, N. Cai, J. Qian, S. Wang, W. Li, H. Wang, *Electrochim. Acta* 88 (2013) 644–653.
- [14] R.J. Kee, M.E. Coltrin, P. Glarborg, *Chemically Reacting Flows*, Wiley, Hoboken, New Jersey, 2003.
- [15] V.M. Janardhanan, O. Deutschmann, *J. Power Sources* 162 (2006) 1192–1202.
- [16] W.G. Bessler, S. Gewies, M. Vogler, *Electrochim. Acta* 53 (2007) 1782–1800.
- [17] A. Bieberle, L.J. Gauckler, *Solid State Ionics* 146 (2002) 23–41.
- [18] V.M. Janardhanan, V. Heuveline, O. Deutschmann, *J. Power Sources* 178 (2008) 368–372.
- [19] Y. Shi, N. Cai, C. Li, C. Bao, E. Croiset, J. Qian, Q. Hu, S. Wang, *J. Electrochem. Soc.* 155 (2008) B270–B280.
- [20] P. Costamagna, P. Costa, V. Antonucci, *Electrochim. Acta* 43 (1998) 375–394.
- [21] S.H. Chan, Z.T. Xia, *J. Electrochem. Soc.* 148 (2001) A388–A394.
- [22] B. Todd, J.B. Young, *J. Power Sources* 110 (2002) 186–200.
- [23] J. Divisek, R. Wilkenh, O. Ner, Y. Volfkovich, *J. Appl. Electrochem.* 29 (1999) 153–163.
- [24] E.S. Hecht, G.K. Gupta, H. Zhu, A.M. Dean, R.J. Kee, L. Maier, O. Deutschmann, *Appl. Catal. A General* 295 (2005) 40–51.
- [25] R.J. Braun, *Optimal Design and Operation of Solid Oxide Fuel Cell Systems for Small-scale Stationary Applications*, Ph.D. thesis, University of Wisconsin, Madison, USA, 2002, pp. 109–111.
- [26] J. Deseure, Y. Bultel, L. Dessemond, E. Siebert, *Electrochim. Acta* 50 (2005) 2037–2046.
- [27] A. Bertei, B. Nucci, C. Nicoletta, *Chem. Eng. Sci.* 101 (2013) 175–190.

## Nomenclature

### Abbreviation

LSM: lanthanum strontium manganite  
RWGS: reverse water gas shift  
ScSZ: scandium stabilized zirconium  
SOEC: solid oxide electrolysis cell  
TPB: triple phase boundary  
WGS: water gas shift  
YSZ: yttrium stabilized zirconium

### English letter

$a$ : pre-exponential factor in sticking coefficient expression  
 $A$ : pre-exponential factor of the Arrhenius form (in terms of cm, mol and s)  
 $b$ : temperature exponent in sticking coefficient expression  
 $c$ : concentration of species (mol m<sup>-3</sup>)  
 $c_{(Ni)}$ : surface concentrations of the free surface active sites on the Ni surface (mol m<sup>-2</sup>)  
 $c_{O(Ni)}$ : surface concentrations of O element on the Ni surface (mol m<sup>-2</sup>)  
 $c_{O^{2-}(YSZ)}$ : the volumetric concentrations of interstitial oxygen in the YSZ ionic conductor (mol m<sup>-3</sup>)  
 $c_{(YSZ)}$ : the volumetric concentrations of interstitial oxygen in the YSZ ionic conductor (mol m<sup>-3</sup>)  
 $c_{O_{bulk}}$ : the oxygen concentrations in the bulk (mol m<sup>-3</sup>)  
 $c_{O_{TPB}}$ : the oxygen concentrations at the TPB (mol m<sup>-2</sup>)  
 $d$ : activation energy in sticking coefficient expression (J mol<sup>-1</sup>)  
 $D^{eff}$ : effective diffusion coefficient (m<sup>2</sup> s<sup>-1</sup>)  
 $D_{Kn}^{eff}$ : effective Knudsen diffusion coefficient (m<sup>2</sup> s<sup>-1</sup>)  
 $D_{mole}^{eff}$ : effective molecular diffusion coefficient (m<sup>2</sup> s<sup>-1</sup>)  
 $E$ : activation energy (kJ mol<sup>-1</sup>)  
 $F$ : Faraday constant (96,384C mol<sup>-1</sup>)

$i_0$ : exchange current density ( $\text{A m}^{-2}$ )  
 $k$ : reaction rate constant (in terms of m, mol and s)  
 $k_{ec}$ : forward electrochemical reaction rate ( $\text{mol m}^{-2} \text{s}^{-1}$ )  
 $k_{-ec}$ : reverse electrochemical reaction rate ( $\text{mol m}^{-2} \text{s}^{-1}$ )  
 $K_g$ : number of gas species  
 $K_s$ : number of surface species  
 $M$ : molecular weight ( $\text{kg mol}^{-1}$ )  
 $n$ : reaction order of the Arrhenius form  
 $n_t$ : total number of electronic and ionic conductor particles  
 $n_{ep}$ : fraction number of electronic conductor particles  
 $n_{ip}$ : fraction number of ionic conductor particles  
 $N$ : number of reactions  
 $p$ : pressure (Pa)  
 $P_{ep}$ : whole range connection probabilities of electronic conductor particles  
 $P_{ip}$ : whole range connection probabilities of ionic conductor particles  
 $\bar{r}$ : average pore radius (m)  
 $r_{ep}$ : mean radius of the electronic conductor particle (m)  
 $R$ : gas constant ( $8.314 \text{ mol}^{-1} \text{ K}^{-1}$ ) or source term of mass balance equation ( $\text{kg m}^{-3} \text{s}^{-1}$ )  
 $S^{eff}$ : effective reaction area per unit volume ( $\text{m}^2 \text{m}^{-3}$ )  
 $S_{Ni}$ : Ni active surface area per unit volume ( $\text{m}^2 \text{m}^{-3}$ )  
 $S_{TPB}$ : TPB active area per unit volume ( $\text{m}^2 \text{m}^{-3}$ )  
 $T$ : temperature (K)  
 $Q$ : current source ( $\text{A m}^{-3}$ )  
 $V$ : diffusion volume or electronic potential (V)  
 $W$ : molecular weight of gas species ( $\text{kg mol}^{-1}$ )  
 $x$ : molar fraction  
 $Z$ : mean coordination number of electron and ionic conductor particles  
 $Z_{ep}$ : coordination number of electron conductor particles  
 $Z_{ip}$ : coordination number of ionic conductor particles

#### Greek letters

$\alpha$ : charge transfer coefficient  
 $\beta$ : cathode electrochemical kinetics parameter  
 $\gamma$ : the sum of all of the surface reactants stoichiometric coefficients  
 $\Gamma$ : surface sites density ( $\Omega^{-1} \text{m}^{-2}$ )  
 $\varepsilon$ : porosity or parameter modeling the species coverage  
 $\eta$ : overpotential (V)

$\theta$ : surface coverage or contact angle between the electronic and ionic conductors (rad)  
 $\mu$ : parameter modeling the species coverage  
 $\nu'$ : stoichiometric coefficient of the reactants  
 $\nu''$ : stoichiometric coefficient of the products  
 $\sigma^{eff}$ : corresponding conductor phase effective conductivity ( $\text{S m}^{-1}$ )  
 $\tau$ : tortuosity  
 $\chi$ : species symbol  
 $\partial\Omega$ : computational domain

#### Subscripts

$ac$ : anode chamber  
 $act$ : active layer  
 $an$ : anode  
 $ca$ : cathode  
 $cccr$ : cathode chamber chemical reactions  
 $ec$ : electrochemical reactions  
 $el$ : electrolyte  
 $elec$ : electronic  
 $ep$ : electronic conductor particle  
 $er$ : electrochemical reactions  
 $i$ : reactions index  
 $g$ : gas phase species  
 $ion$ : ionic  
 $ip$ : ionic conductor particle  
 $Kn$ : Knudsen  
 $mole$ : molecular  
 $ref$ : reference  
 $sp$ : support layer  
 $t$ : total

#### Superscripts

$0$ : parameter at equilibrium conditions  
 $bulk$ : bulk phase  
 $eff$ : effective  
 $TPB$ : triple phase boundary